Crystal Structures of Mutant *Pseudomonas aeruginosa* *p*-Hydroxybenzoate Hydroxylases: The Tyr201Phe, Tyr385Phe, and Asn300Asp Variants†

Myoung Soo Lah,‡ Bruce A. Palfey, Herman A. Schreuder,§ and Martha L. Ludwig*

Department of Biological Chemistry and Biophysics Research Division, University of Michigan, Ann Arbor, Michigan 48109

Received July 15, 1993; Revised Manuscript Received November 3, 1993®

ABSTRACT: Structures of the mutant *p*-hydroxybenzoate hydroxylases, Tyr201Phe, Tyr385Phe, and Asn300Asp, each complexed with the substrate *p*-OHB have been determined by X-ray crystallography. Crystals of these three mutants of the *Pseudomonas aeruginosa* enzyme, which differs from the wild-type *Pseudomonas fluorescens* enzyme at two surface positions (228 and 249), were isomorphous with crystals of the wild-type *P. fluorescens* enzyme, allowing the mutant structures to be determined by model building and refinement, starting from the coordinates for the oxidized *P. fluorescens* PHBH–3,4-diOHB complex [Schreuder, H. A., van der Laan, J. M., Hol, W. G. J., & Drenth, J. (1988) *J. Mol. Biol. 199*, 637–648]. The *R* factors for the structures described here are: Tyr385Phe, 0.178 for data from 40.0 to 2.1 Å; Tyr201Phe, 0.203 for data from 40.0 to 2.3 Å; and Asn300Asp, 0.193 for data from 40.0 to 2.3 Å. The functional effects of the Tyr201Phe and Tyr385Phe mutations, described earlier [Entsch, B., Palfey, B. A., Ballou, D. P., & Massey, V. (1991) *J. Biol. Chem. 266*, 17341–17349], were rationalized with the assumption that the mutations perturbed the hydrogen-bonding interactions of the tyrosine residues but caused no other changes in the enzyme structure. In agreement with these assumptions, the positions of the substrate, the flavin, and the modified residues are not altered in the Tyr385Phe and Tyr201Phe structures. In contrast, substitution of Asp for Asn at residue 300 has more profound effects on the enzyme structure. The side chain of Asp300 moves away from the flavin, disrupting the interactions of the carboxamide group with the flavin O(2) atom, and the α-helix H10 that begins at residue 297 is displaced, altering its dipole interactions with the flavin ring. The functional consequences of these changes in the enzyme structure and of the introduction of the carboxyl group at 300 are described and discussed in the accompanying paper (Palfey et al., 1994b).

The flavoprotein hydroxylases, of which *p*-hydroxybenzoate hydroxylase (PHBH,[1] EC 1.14.13.2) is the best-studied example, catalyze the monooxygenation of activated aromatic compounds, utilizing flavin 4a-hydroperoxides as intermediates. The reaction cycle for PHBH, established by stopped flow and other kinetic techniques, is shown in Scheme 1 [Entsch et al., 1976; Wessiak et al., 1984; Entsch & Ballou, 1989; reviewed in Palfey et al. (1994a)]. Key steps in the mechanism are as follows: (1) the facilitation by bound substrate of the reduction of the FAD prosthetic group and (2) the hydroxylation of substrates, which is believed to proceed by electrophilic substitution (Palfey et al., 1994a). Uncoupling of hydroxylation from reoxidation of the flavin ring system, yielding peroxide as a product, occurs with certain poor substrates or analogues and can be enhanced by mutation of residues in the active center.

Site-directed mutagenesis has been employed by Entsch et al. (1991) and by van Berkel and colleagues (van Berkel et al., 1992) to examine the roles of active-center residues in catalysis. The choice of mutation sites has been based on the three-dimensional structure of PHBH from *Pseudomonas fluorescens* (Wierenga et al., 1979; Schreuder et al., 1989). Structural data for two TyrPhe mutants of PHBH from *P. aeruginosa* (Entsch et al., 1988) are presented in this paper. Tyrosines 201 and 385, replaced by phenylalanine in separate mutagenesis experiments, are part of a hydrogen-bonding network that includes the 4-OH of bound substrate (Figure 1). Mutation of either of these residues to phenylalanine decreases the maximum turnover of NADPH by factors of 15–40 (Entsch et al., 1991). In the Tyr201Phe and Tyr385Phe mutants, the rate of reduction of the enzyme–substrate complex by NADPH decreases 10-fold and 100-fold, respectively. Reoxidation of reduced flavin is markedly uncoupled from hydroxylation in the Tyr201Phe mutant, and the rate constant for the hydroxylation step (k_3 of Scheme 1) is decreased by a factor of approximately 1000 in this mutant. In contrast, hydroxylation by the Tyr385Phe mutant accounts for 75% of the NADPH consumed and proceeds with a rate constant about one-tenth that observed for wild-type enzyme. Comparisons of these and other properties of wild-type and of Tyr201Phe and Tyr385Phe mutants have suggested that hydrogen bonding between the hydroxyl group of Tyr201 and the 4-OH of the substrate is important in activating *p*-OHB for electrophilic attack by the distal oxygen of the flavin hydroperoxide (Entsch et al., 1991; Palfey et al., 1994a). The structure analyses of the two Tyr mutants support this interpretation. The positions of the flavin, substrate, and aromatic residues are essentially the same as found in wild-type enzyme, but hydrogen-bonding interactions of the tyrosine hydroxyl groups are lost and not replaced.

The accompanying paper (Palfey et al., 1994b) describes in detail the kinetic and other properties of another mutant

† Supported by grants from NIH (GM 16429 to M.L.L. and GM 20877 to D. P. Ballou), Michigan Molecular Biophysics Training Program (GM 08270, B.A.P.), and a Rackham Graduate School Predoctoral Fellowship (B.A.P.).

* To whom correspondence should be addressed at: Biophysics Research Division, University of Michigan, 930 N. University Ave., Ann Arbor, MI 48109-1055.

‡ Present address: Department of Chemistry, Hanyang University, 396 Taehakdong Ansan, Kyunggido, Korea.

§ Present address: Marion Merrell Dow Research Institute, 16 Rue d'Ankara, 67046 Strasbourg Cedex, France.

® Abstract published in *Advance ACS Abstracts,* January 15, 1994.

[1] Abbreviations: PHBH, *p*-hydroxybenzoate hydroxylase; *p*-OHB, *p*-hydroxybenzoate; 3,4-diOHB, 3,4-dihydroxybenzoate; E_{ox}, enzyme with FAD in the oxidized form; $FADH^-$, the anionic form of reduced FAD; WT, wild-type PHBH.

0006-2960/94/0433-1555$04.50/0

Scheme 1: Reaction Cycle for PHBH, Based on Stopped-Flow Kinetic Analyses[a]

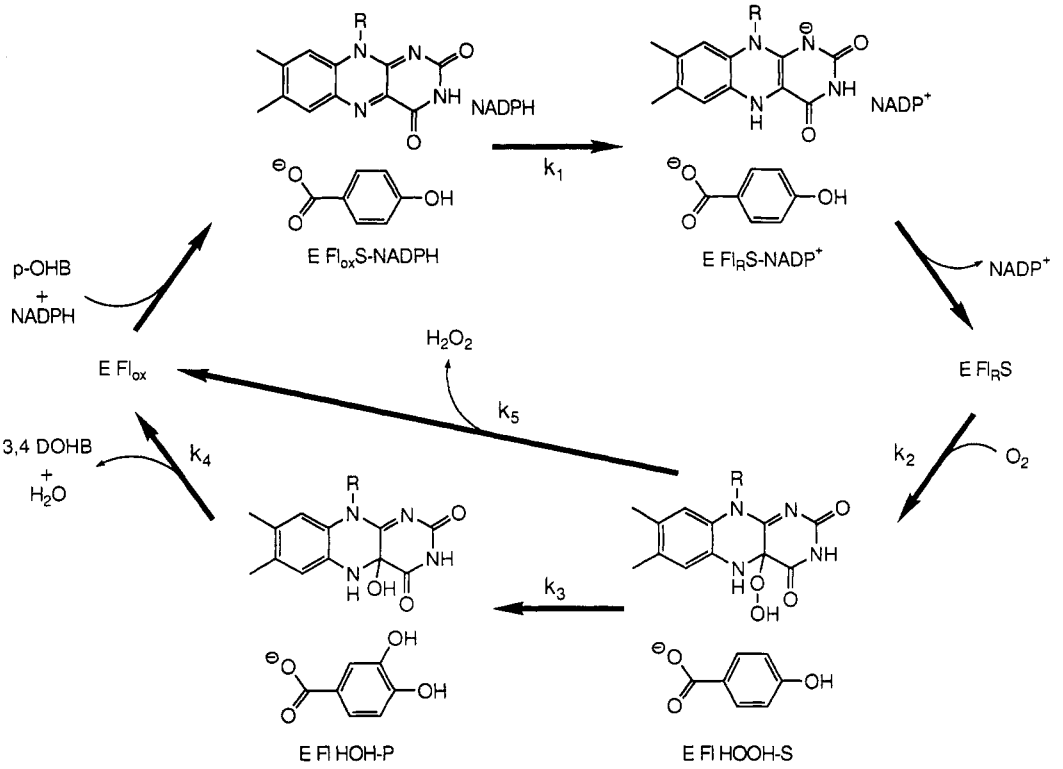

[a] The step with rate constant k_1 is the reduction of the flavin in the presence of substrate; k_2 refers to the formation of the 4a-flavin hydroperoxide species, k_3 refers to the substrate hydroxylation, and k_4 refers to the dehydration of the flavin 4a-hydroxide (Entsch et al., 1976; Palfey et al., 1994a). Uncoupling occurs via step 5. The abbreviations used are as follows: EFlHOOH, C(4a)-hydroperoxide of the enzyme-bound FAD; EFlHOH, C(4a)-hydroxide of the enzyme bound FAD.

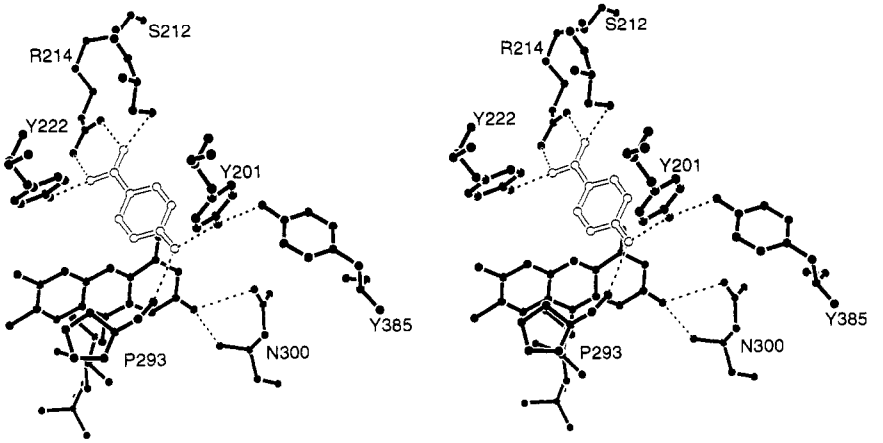

FIGURE 1: Active site of oxidized wild-type *P. fluorescens* PHBH, complexed with *p*-OHB. Coordinates are from the structure described by Schreuder et al. (1989). The view is chosen to display the hydrogen bonds which position the bound substrate (drawn with open bonds) and connect substrate with Tyr201 and Tyr385 (see Table 3). The network of hydrogen bonds connecting substrate and tyrosines lies on the *re* side of the flavin ring but extends toward the surface at His72 in a direction opposite to the presumed pathway for approach of substrate (Schreuder, 1988).

PHBH, Asn300Asp. Asn300 is the only side chain in the wild-type structure that hydrogen bonds to the isoalloxazine ring; it is therefore likely to affect the electronic properties of the flavin. As reported by Palfey et al. (1994b), the turnover number (TN) for this mutant is decreased by a factor of 100, relative to that of wild-type enzyme at pH 6.5. The mutation affects both the reductive and oxidative half-reactions, with decreases of 50–100-fold in the rates of hydroxylation and of conversion of the flavin 4a-OH to oxidized flavin, respectively, and lowers the two-electron redox potentials by 20–40 mV. The structure analysis has been important in rationalizing these properties since the mutation is not a simple replacement of $-COO$ for $-CONH_2$ but results in additional changes in the positions of protein and solvent atoms.

MATERIALS AND METHODS

Preparation of Mutant Enzymes. Mutant strains of *pobA* were generated as described (Entsch et al., 1991; Palfey et al., 1994b). Purification of the Asn300Asp mutant utilized a modified procedure, described in the accompanying paper (Palfey et al., 1994b), which relies on the ability of the dye, red A, to displace FAD from the hydroxylase protein. Each mutant protein was further purified for crystallization by FPLC on a mono-Q column, using a Na_2SO_4 gradient in 10 mM Tris sulfate, pH 7.5.

Table 1: Summary of Data Sets and Crystallographic Structures

	Y385F	Y201F	N300D
crystal size (mm)	0.28 × 0.84 × 0.54[a]	0.10 × 0.75 × 0.40	0.12 × 0.50 × 0.26
space group	$C222_1$	$C222_1$	$C222_1$
cell parameters (Å)	a = 71.78	a = 71.71	a = 71.88
	b = 146.53	b = 146.27	b = 146.62
	c = 88.28	c = 87.91	c = 88.27
resolution range (Å)	40.0–2.1	40.0–2.3	40.0–2.3
unique reflections	26 888	20 499	20 384
completeness (%)	97	98	97
redundancy	4.3	4.0	4.1
R_{sym} (%)[b]	6.77	12.30	12.06
av $I/\sigma(I)$	11.4	6.63	5.28
initial model	Schreuder et al. (1988)	Y385F	Y385F
final R factor	0.178	0.203	0.193
no. of water molecules	191	179	151

[a] Crystal 1. The volume of the second crystal was smaller by about 20%. [b] Calculated with intensities, using deviations from $\langle I \rangle$.

Crystals and Data Collection. All mutant proteins from *P. aeruginosa* were crystallized as the substrate complexes ($PHBH_{ox}$–*p*-OHB) using free interface diffusion in sealed capillary tubes as described for wild-type PHBH from *P. fluorescens* (Drenth et al., 1975; van der Laan et al., 1989). With ammonium sulfate as the precipitant, crystals nucleate at pH 7.5 in 0.1 M phosphate buffer as the temperature is raised from 4 °C. The crystals are orthorhombic, space group $C222_1$, a = 71.7–71.9, b = 146.3–146.6, and c = 87.9–88.3 Å, with the monomer chain of 394 residues constituting the asymmetric unit. The data sets used for refinements of the mutant structures were collected with a SDMS dual area detector at room temperature, using two crystals for the Tyr385Phe data set and one crystal for each of the other data sets. The resolution limit was 2.3–2.1 Å, depending on the mutant. A summary of the X-ray measurements is presented in Table 1. The R_{sym} values for the Tyr385Phe measurements are in the range expected for area detector data but are relatively large for the Tyr201Phe and Asn300Asp crystals, whose scattering volumes were one-fourth to one-eighth that of the larger Tyr385Phe crystal. R_{sym} as a function of intensity was similar in all three data sets. However, the R_{sym} values increased more rapidly with resolution for the smaller crystals, exceeding 13.5% and 14.5% at resolutions greater than 3.1 Å in the Asn300Asp and Tyr201Phe data sets, respectively.

Structure Analysis by Refinement and Model Building. The atomic structures of the mutants were derived from the structure of the wild-type enzyme by alternating cycles of refinement using X-PLOR (Brünger et al., 1990; Brünger, 1992) with model building. Coordinates were adjusted as indicated by electron densities in maps with amplitudes ($|F_o| - |F_c|$) or ($|2F_o| - |F_c|$), using the program TOM (Cambillau & Horjales, 1987). The first data to be analyzed were from the Tyr385Phe mutant. The structure of *P. aeruginosa* Tyr385Phe was the starting point for subsequent refinement of the other mutants. Each round of refinement and modeling is designated by a letter code in Table 2.

The first calculation for each mutant was a rigid body adjustment of the protein model in the unit cell. Subsequent steps used minimization by positional refinement (30–120 cycles) and in some rounds employed simulated annealing from 1000 K (Brünger et al., 1990). Isotropic atomic temperature factors were adjusted for at least 20 cycles after positional refinements. Solvents were added to the models after the initial rounds whenever they corresponded to densities of 3σ in difference maps and formed acceptable interactions with protein atoms. In later rounds, solvents were added using the same criteria or were removed from coordinate lists if their temperature factors exceeded 50.0 Å^2. In the last stages of each refinement, all measured reflections were included, and the scattering contributions of bulk solvent were estimated using scale and temperature factors according to Brünger (1992). The coordinates from the refinements of the three mutant structures will be deposited in the Protein Data Bank.

Parameters for the isoalloxazine ring of FAD were refined with restraints similar to those employed by Schreuder et al. (1989) in the refinement of PHBH–*p*-OBH, which used the programs developed by Hendrickson and Konnert (Hendrickson, 1985). In the present studies, the benzene and the pyrimidine moieties of the isoalloxazine ring were restrained to maintain planarity, but the nitrogen atoms N(5) and N(10) of the central ring were not required to adopt sp^2 geometry. This parametrization allowed for twisting and folding of the flavin ring and permitted comparison with the ring parameters derived for various redox states and liganded species of the *P. fluorescens* enzyme.

Refinement of the Tyr385Phe–p-OHB Structure. The space group of the crystals, $C222_1$, is identical to that of the wild-type PHBH–3,4-DOHB and wild-type PHBH–*p*-OHB complexes. The unit cell parameters of the crystal of the Tyr385Phe–*p*-OHB mutant (Table 1) differed slightly from those of crystals of wild-type *P. fluorescens*, reported to be a = 71.5, b = 145.8, and c = 88.2 Å by Schreuder et al. (1989). Coordinates for the product complex of wild-type enzyme (PHBH–FAD–3,4-diOHB) at 2.3-Å resolution, 1PHH from the Protein Data Bank (Schreuder et al., 1988), provided the starting model for refinement. The sequence of computations is summarized in Table 2. Rigid body refinement of the starting model, excluding substrate and solvents, decreased R from 0.426 to 0.339. Subsequent positional refinement and simulated annealing (round A of Table 2) reduced the R value to 0.223. Density corresponding to the substrate, *p*-OHB, was well-defined in ($|2F_o| - |F_c|$) and ($|F_o| - |F_c|$) maps. After manual adjustment and inclusion of three carboxyl terminal residues and 274 solvents, positional refinement was repeated at step B. Although the R value after step B was 0.210 for data from 5.0 to 2.1 Å with $F > 2\sigma(F)$, electron densities in several regions remained difficult to interpret and were not modeled satisfactorily by the 1PHH coordinates. At this stage, major revisions of the model were made at residues 43–44, 60–62, 80–82, 143–145, 191–197, 248–254, 262–267, and 297–298. Four subsequent rounds of refinement and manual adjustments decreased R from 0.238 to 0.173. ($|2F_o| - |F_c|$) and ($|F_o| - |F_c|$) maps after step F verified the placement of backbone and side-chain atoms in regions that had been ambiguous. At step G, the data from 5.0 to

Table 2: Crystallographic Refinements

run	resol (Å)	reflections used (total)[b]	atoms (inc. polar H)	no. of solvents	calcd[c]	R_{init}	R_{final}
			Tyr385Phe[a]				
A	5.0–2.1	23 105 (24 593)	3907	0	R	0.426	0.339
					P	0.356	0.288
					PSB	0.305	0.223
B	5.0–2.1	23 105 (24 593)	4640	274	P	0.246	0.210
C	5.0–2.1	23 105 (24 593)	3918	0	PB	0.238	0.205
D	5.0–2.1	23 105 (24 593)	3918	0	PB	0.214	0.200
E	5.0–2.1	23 105 (24 593)	4227	103	PB	0.194	0.176
F	5.0–2.1	23 105 (24 593)	4218	100	PB	0.180	0.173
G	40.0–2.1	25 216 (26 733)	4323	135	PB	0.196	0.185
H	40.0–2.1	25 216 (26 733)	4407	163	PB	0.186	0.181
I	40.0–2.1	25 216 (26 733)	4533	205	PB	0.185	0.172
J	40.0–2.1	25 216 (26 733)	4530	204	PB	0.174	0.173
K	40.0–2.1	26 733	4530	204	PB	0.183	0.183
L	40.0–2.1	26 733	4540[d]	205	PB	0.181	0.180
					Bocc	0.186	0.189
					B	0.184	0.180
M	40.0–2.1	26 733	4498[d]	191	P	0.182	0.182
					PSB	0.182	0.178
			Tyr201Phe[a]				
A	10.0–2.7	11 324 (12 524)	3918	0	R	0.266	0.230
	6.0–2.3	15 558 (18 671)	3918	0	PB	0.237	0.201
B	6.0–2.3	15 558 (18 671)	4533	205	PB	0.188	0.165
	40.0–2.3	16 809 (19 561)	4533	205	PB	0.184	0.183
C	40.0–2.3	16 809 (19 561)	4395	159	PB	0.191	0.185
D	40.0–2.3	19 561	4443	175	PB	0.212	0.204
E	40.0–2.3	19 561	4455	179	PB	0.204	0.203
			Asn300Asp[a]				
A	10.0–2.7	11 812 (12 285)	3918	0	R	0.290	0.253
	6.0–2.3	16 346 (17 886)	3918	0	PB	0.258	0.203
					PSB	0.203	0.188
B	6.0–2.3	16 346 (17 886)	4455	179	PB	0.192	0.173
C	40.0–2.3	19 094	4368	150	P	0.205	0.200
					PSB	0.200	0.190
D	40.0–2.3	19 094	4398	160	P	0.193	0.195
					PSB	0.195	0.191
E	40.0–2.3	19 094	4371	151	P	0.194	0.194
					PSB	0.194	0.193
F	15.0–2.3	18 965	4371	151	PB	0.205	0.185
	10.0–2.3	18 762	4371	151	PB	0.184	0.183

[a] 3124 non-hydrogen protein atoms, 53 FAD, and 10 substrate atoms in the Tyr mutants; 3125 protein atoms in the Asn mutant. [b] When observed reflections were not used, the cutoff was at $F < 2\sigma(F)$. [c] Modes of computation are R, rigid-body refinement; P, positional refinement; S, simulated annealing; B, individual temperature factor refinement; Bocc, refinement of group B's and occupancies of solvents. [d] Includes an alternate conformation for the ring of His197.

40.0 Å were incorporated and a bulk solvent correction was applied (Brünger, 1992), and at step K all data were included in the refinement. The final R factor was 0.178 for all data in the 40.0–2.1-Å resolution range. The average temperature factor for the protein (including bound solvents) was 15.5 Å^2; the overall B determined from Wilson plots of data between 4.0 and 2.3 Å was 21.9 Å^2.

At the conclusion of the refinement, analysis of the ϕ and ψ angles showed that the angles for Arg44 lie in a 'disallowed' region of the Ramachandran plot. This residue adjoins the flavin and is well-ordered. Its unusual conformation has been verified in omit maps by Schreuder et al. (1989). The electron densities at the two residues, Ser228 and Ser249, in *P. aeruginosa* that are different from *P. fluorescens* (Thr and Ala, respectively) confirmed their identities.

Retrospective comparison with coordinates from the refinement of *P. fluorescens* PHBH–*p*-OHB at 1.9 Å showed that the revisions of the 1PHH model made during refinement of the Tyr385Phe mutant were very similar to the revisions of the wild-type structure made independently by Schreuder et al. (1989). The backbone of the model for the Tyr385Phe mutant differs somewhat from the model of Schreuder et al. (1989) at the chain termini and at residues 80, 133, 144–145, and 354–355. At the internal sites, the peptide orientations have been assigned differently in the two models. The most significant variation is the choice of a type II turn at Asp144: Gly145 in Tyr385Phe; this turn is type I in the model for wild-type PHBH.

Refinement of the Tyr201Phe–p-OHB Structure. Refinement started with the final coordinates for the protein atoms of the mutant Tyr385Phe. The initial R value for data between 10.0 and 2.7 Å resolution with amplitudes greater than $2\sigma(F)$ decreased to 0.230 after rigid-body refinement. Subsequent positional refinement and isotropic temperature factor refinement for data in the 6.0–2.3-Å resolution range reduced the R value to 0.201. ($|2F_o| - |F_c|$) and ($|F_o| - |F_c|$) maps after step A indicated sites for 205 solvent molecules. After the extension of low-resolution data to 40.0 Å and model building in rounds B and C, all measured data were incorporated for rounds D and E. The final R factor was 0.203 for all data in the 40.0–2.3-Å resolution range. The average temperature factor for protein and defined solvent atoms was 13.1 Å^2, compared to an overall B of 15.7 Å^2 determined from Wilson plots of data between 4.0 and 2.3 Å resolution.

Refinement of the Asn300Asp–p-OHB Structure. The structure of the mutant Asn300Asp was refined starting with the final coordinates for the mutant Tyr385Phe. The R value for data between 10.0 and 2.7 Å with $F > 2\sigma(F)$ was 0.253

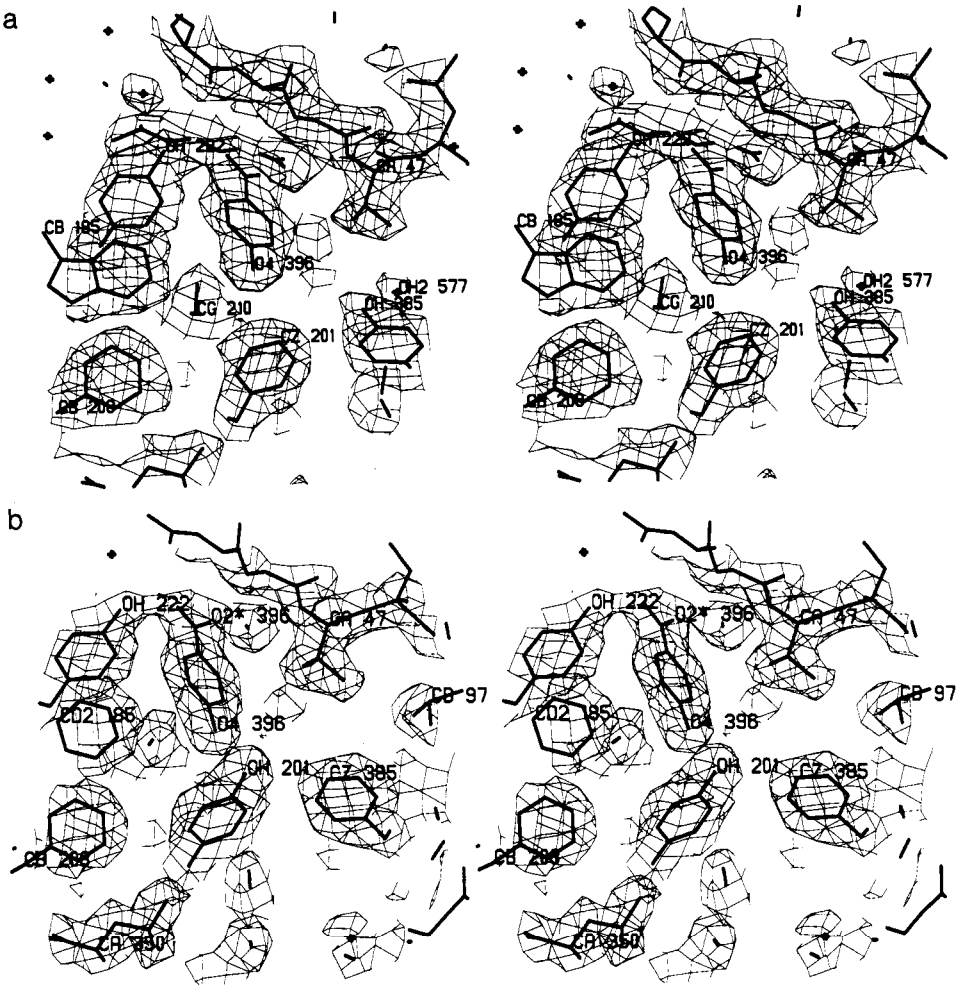

FIGURE 2: Electron density maps of the TyrPhe mutants. (a) ($|2F_o| - |F_c|$) map of the mutant Tyr201Phe in the vicinity of Phe201. Contours corresponding to the substrate (residue 396) and to tyrosines 222 and 385 can be compared with the density defining the phenylalanine ring at 201 and with the equivalent map for the Tyr385Phe mutant shown in panel b. Density corresponding to the solvent that interacts with Tyr385 can be seen at the lower right, and the edge of the flavin ring is visible behind the substrate. ($|F_o| - |F_c|$) maps at 3σ are featureless in the vicinity of the mutation. (b) A ($|2F_o| - |F_c|$) map in the vicinity of Phe-385 in the mutant Tyr385Phe. The center and perspective are shifted slightly from panel a.

after rigid-body refinement. Because of the significant shifts in structure in the vicinity of the mutation, simulated annealing was alternated with positional refinement to develop the revised model. Difference maps at the end of round A revealed the altered position of the side chain at residue 300 and the shifts of residues comprising the start of α-helix H10, along with changes in the positions of several other side chains (cf. Figure 6). After the rebuilding and inclusion of solvents, four additional rounds of refinement led to an R of 0.193 for all data between 40.0 and 2.3 Å resolution. Root mean square deviations from ideal bond lengths and angles were 0.019 Å and 1.5°.

The effects of including inner data were investigated with this mutant on account of its small temperature factors. The low-resolution cutoff was set at 15.0 and then at 10.0 Å (Table 2). In each case positional, overall B, and individual B values were refined in alternating fashion. Using data between 15.0 or 10.0 and 2.3 Å, the average B for the protein and solvent atoms converged to 8.4 Å^2, compared to an overall B of 12.6 Å^2 determined from Wilson plots of data between 4.0 and 2.3 Å. With data between 40.0 and 2.3 Å, the average B was found to be 7.8 Å^2.

The temperature factors for the several mutants differ significantly, with those for the Asn300Asp mutant being consistently small and those for Tyr385Phe larger, although the protocols for data collection and the extents of decay from radiation damage were similar for all the structures reported here.[2] Direct comparison of the F_{obs} data confirms that the overall temperature factor for the crystal of the Asn300Asp mutant is smaller by about 9 Å^2 than that for the Tyr385Phe mutant. The variation of temperature factors along the sequence is the same as in the structures of the Tyr385Phe or Tyr201Phe mutants.

RESULTS

Structures of Mutants Tyr201Phe and Tyr385Phe, in Complexes with Substrate (PHBH$_{ox}$-p-OHB). These TyrPhe mutations of *P. aeruginosa* PHBH produce only small changes in the structure of the enzyme (Figures 3 and 4). The rms deviation of the Cα atoms from the structure of wild-type *P. fluorescens* PHBH (Schreuder et al., 1989) is 0.30 Å for Tyr201Phe and 0.29 Å for Tyr385Phe. The positions and orientations of the aromatic rings at the sites of mutation are maintained, and the flavin ring retains the slight twist that has been described for the oxidized wild-type structure. The same sense and approximate magnitude of ring twist is observed in the Tyr201Phe, Tyr385Phe, and wild-type PHBH structures even though completely different refinement algorithms were

[2] Decay was determined by remeasuring some of the initial data and averaged 16–22% at the conclusion of data collection.

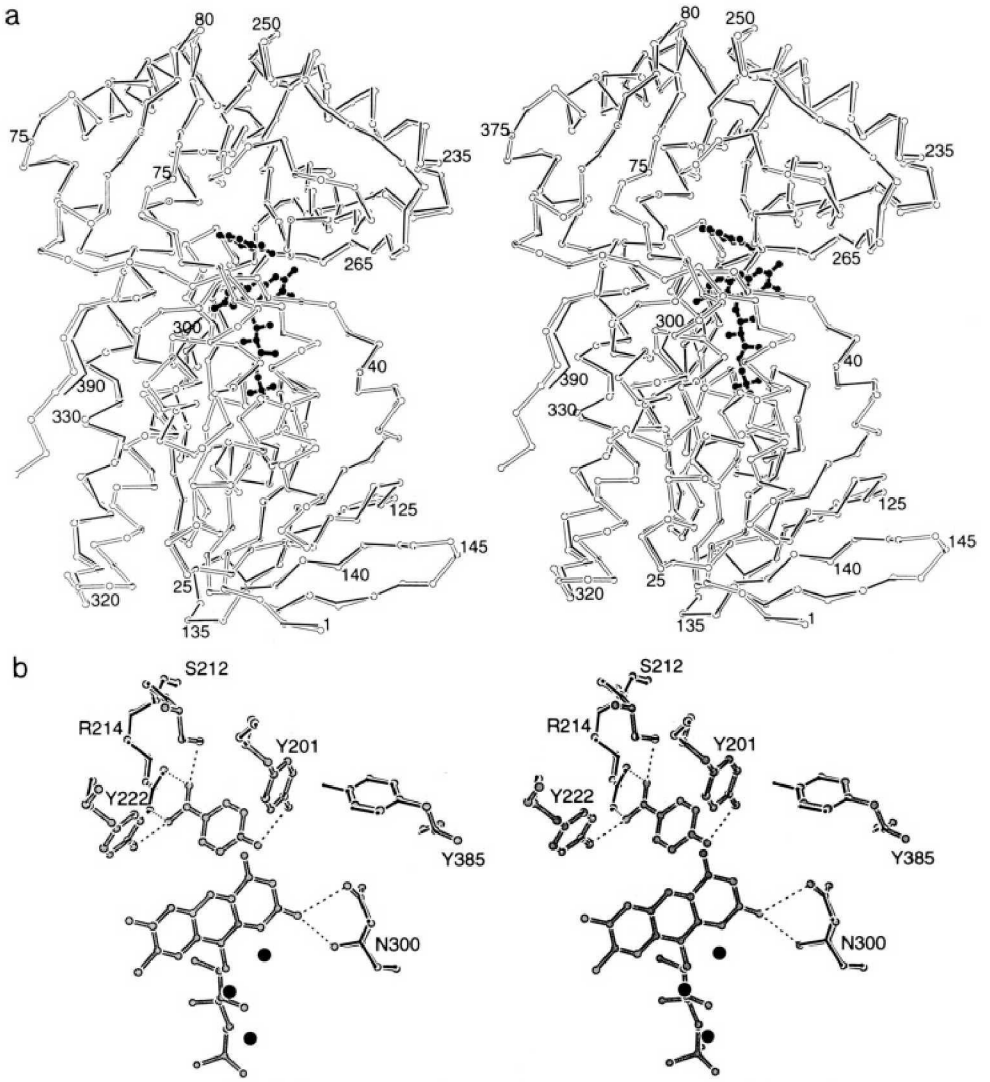

FIGURE 3: Structure of the mutant Tyr385Phe. (a) Superposition of the Cα backbones of wild-type PHBH from *P. fluorescens* (Schreuder et al., 1989) and the Tyr385Phe mutant of PHBH from *P. aeruginosa*. The structure of wild-type enzyme is drawn with solid bonds and the mutant with open bonds. FAD and substrate (thick filled bonds) are included for comparison with other figures. After refinement, the rms deviation of the backbone coordinates of mutant and wild-type enzymes is 0.29 Å. Residue differences which distinguish the strains of *Pseudomonas* occur at positions 228 and 249. Differences of main-chain positions are found at the N- and C-terminus and at residues 80, 133, 144, and 354–355. Variations between wild-type and the other mutants are even smaller, but in each of the mutant structures reported here the turn at Asp144:Gly145 has been built as type II, whereas this turn is type I in the model of wild-type PHBH. (b) Superposition of the active centers of wild-type *P. fluorescens* PHBH and the *P. aeruginosa* mutant Tyr385Phe in the same orientation as Figure 1. The wild-type structure is represented by thin bonds and the mutant by thicker gray bonds. For clarity, the substrate and flavin atoms of wild-type enzyme have been omitted. Dashed lines indicate the hydrogen bonds deduced from coordinates of the structure of the mutant.

used in the structure analyses of the mutant and wild-type enzymes. Some variations in the orientations of Leu210 and Val75, residues that pack against Tyr201 and Tyr385, appear after refinement, but the orientations of these side chains can be difficult to define at resolutions of 2.1–2.3 Å.

The electron density maps corroborate the deletion of the hydroxyl groups from Tyr201 or Tyr385 (Figure 2). Loss of the hydrogen-bonding capacity of these groups (Figures 3b and 4) dictates changes in the hydrogen-bonding network that extends from the substrate toward the surface of the molecule. In the wild-type enzyme–substrate complex (Figure 1), the predominant species is expected to be the form in which Tyr201 OH serves as hydrogen-bond donor to the substrate phenol or phenolate group while the 4-OH of Tyr385 OH serves as donor to Tyr201. Deletion of the hydroxyl group at 201 removes the hydrogen-bond donor to the substrate and breaks the connection between the substrate and Tyr385. In the Tyr201Phe mutant, a prominent solvent peak is found on the opposite side of the 4-OH of Tyr385 (Figures 2a and 4), suggesting that in the mutant the phenol group of Tyr385 rotates to form a hydrogen bond to this solvent. The hydrogen-bonding interactions of wild-type and mutant enzymes, deduced from the structure, are compared in Table 3.

Structure of the Mutant Asn300Asp, in a Complex with Substrate (PHBH$_{ox}$–p-OHB). Significant structural changes are observed in the vicinity of the mutation (Figure 5). Residue 300 is located near the start of the long α-helix H10 that is proposed to stabilize the reduced form of FAD, FADH$^-$ (Vervoort et al., 1991), by dipole interactions (Hol et al., 1978) with the isoalloxazine ring. In wild-type PHBH, the Asn side chain interacts with the isoalloxazine O(2) and with backbone atoms of residues 47, 49, and 296 (Table 4). In the Asp mutant structure described here, the side chain has moved away from the isoalloxazine ring; the carboxyl carbon of residue 300 is displaced by about 5 Å from its position in the wild-type structure (Figure 6). The Asp300 side chain perturbs the local environment around its new position: residues Glu49, Arg335, and Tyr390 move slightly, waters (574 and 558) are displaced to make room for the side chain, and a new hydrogen bond forms between Lys297 and a carboxylate oxygen of

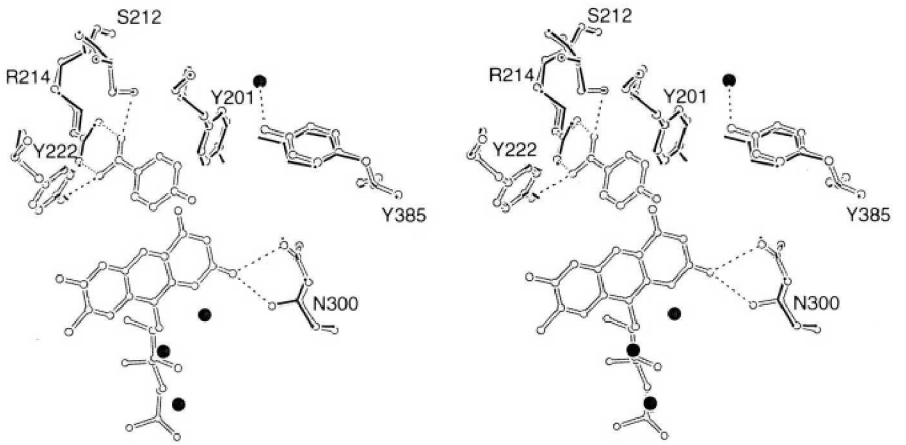

FIGURE 4: Structure of the mutant Tyr201Phe. A superposition of the active centers of mutant and wild-type enyzmes, with the same conventions as in Figure 3b. In the Tyr201Phe mutant, a solvent is observed at a position where it can accept a hydrogen bond from the 4-OH of Tyr385. This water (filled) completes a network of hydrogen bonds that connects Tyr385 with His72, a residue at the surface of the molecule.

Table 3: Polar Interactions of Substrate and of Tyrosines 201 and 385

			distance (Å)			
target	atom	neighbor	wild type	Y385F	Y201F	N300D
p-OHB[a]	O2*	Ser 212 OG1	2.75	2.76	2.78	2.82
		Arg 214 NH2	2.83	2.84	2.95	2.85
		Arg 214 NH1		3.56	3.64	3.33
	O1*	Tyr 222 OH	2.33	2.67	2.75	2.69
		Arg 214 NH1	3.07	2.94	3.01	2.86
	O4	Pro 293 O	2.92	2.80	2.86	2.71
		Tyr 201 OH	2.67	2.80		2.88
201	OH	Tyr 385 OH	2.81			2.86
385	OH	Wat 577			2.85	

[a] Labels of *p*-OHB carboxylate oxygens are opposite to those in Schreuder (1989).

Asp300. The carboxyl group of Asp300 is assumed to be ionized in the cluster of charges that includes Arg335, Lys297, and Glu49. It is tempting to surmise that the structural changes observed in crystals at pH 7.5 are the result of optimizing electrostatic interactions between the protein and the ionized Asp300 side chain.

Movement of the side chain of residue 300 appears to be coordinated with significant shifts in the backbone of α-helix H10, which is displaced by approximately 1.5 Å at the Cα of residue 300. These shifts alter the local dipole interactions of the backbone peptides with the flavin (Aqvist et al., 1991; He & Quiocho, 1993). In particular, the NH groups of residues 299 and 300 move with respect to the flavin N(1) and O(2) atoms, and the hydrogen bond between NH 300 and O(2) is broken (Table 4 and Figure 6). The vacancy created by the movement of Asp300 is occupied by two water molecules. Substitution of these solvents provides a hydrogen-bonding environment near the flavin that is similar but not identical to that of wild-type PHBH (Figure 6 and Table 4).

DISCUSSION

Structure–Function Correlations from Studies of the Mutants Tyr201Phe and Tyr385Phe. Kinetic analyses of the Tyr201Phe and Tyr385Phe mutants, combined with studies of the interactions of substrates and substrate analogs (Entsch et al., 1991), have related several properties of PHBH to the presence of the hydrogen-bond network connecting residues 385, 201, and the bound substrates, *p*-OHB (see Figures 3b and 4). The decreased rate of hydroxylation (denoted by k_3 in Scheme 1) in the mutants Tyr201Phe and Tyr385Phe has suggested that the intact network of hydrogen bonds in wild-type PHBH assists in activation of substrate for attack by the terminal OH of the flavin 4a-hydroperoxide (Entsch et al.,

Table 4: Polar Interactions near Residue 300 in Wild Type and N300D

wild-type PHBH					N300D mutant PHBH				
atom	residue	atom	residue	dist (Å)	atom	residue	atom	residue	dist (Å)
ND2	Asn 300	O(2)	FAD 395	3.15	O	Wat 550	O(2)	FAD 395	3.60
		O	Val 47	2.81			O	Val 47	3.27
		O	Ala 296	2.95			O	Ala 296	2.73
		N	Glu 49	3.45			N	Glu 49	3.46
OD1	Asn 300	O(2)	FAD 395	4.53	O	Wat 551	O(2)	FAD 395	4.56
		N	Glu 49	2.96			N	Glu 49	2.96
		OE2	Glu 49	4.51			OE2	Glu 49	3.29
N	Asn 300	O(2)	FAD 395	3.11	N	Asp 300	O(2)	FAD 395	4.02
NZ	Lys 297	OE1	Glu 49	2.84	NZ	Lys 297	OD2	Asp 300	3.11
		O	Tyr 385	2.85			O	Tyr 385	3.25
		O	Tyr 384	3.25			O	Tyr 384	3.21
O(2)	FAD 395	O	Ala 296	3.35	O(2)	FAD 395	O	Ala 296	3.05
		N	Lys 299	2.95			N	Lys 299	2.91
O(4)	FAD 395	N	Gly 46	3.10	O(4)	FAD 395	N	Gly 46	3.07
		N	Val 47	3.13			N	Val 47	3.26
N(3)	FAD 395	O	Val 47	2.91	N(3)	FAD 395	O	Val 47	2.91
					OD1	Asp 300	NH1	Arg 335	3.24
							NH2	Arg 335	2.70
							OE1	Glu 49	3.16
					OD2	Asp 300	NZ	Lys 297	3.11
							O	Wat 458	3.50

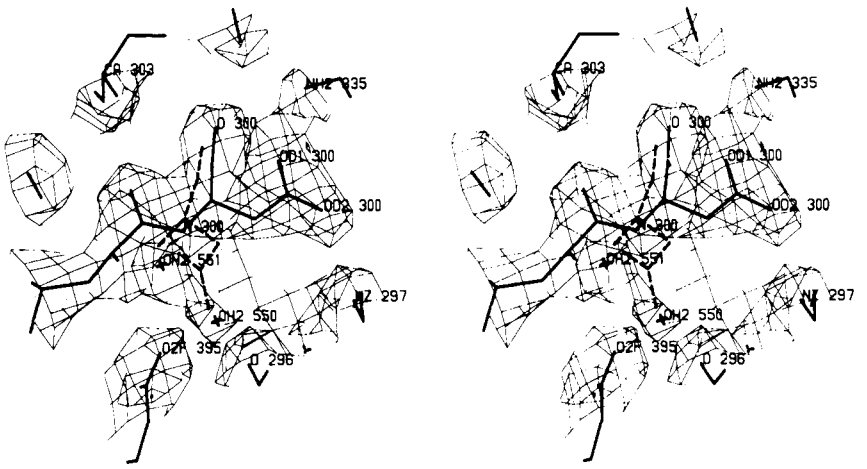

FIGURE 5: Structure of the mutant Asn300Asp in the vicinity of the mutation. Electron density (thin contours) is from a ($|2F_o| - |F_c|$) map computed at the end of the refinement. For comparison, the position of Asn300 in the wild-type structure is represented in dashed bold lines. Density which corresponds to the solvents that are substituted for the carboxamide O and N atoms is evident in this view. The perspective is similar to that used for the drawings of Figure 6.

Table 5: Some Properties of Wild-Type and Mutant Hydroxylases

	relative activity (TN, s^{-1})					E'_o (mV)	
enzyme	pH 7.9	pH 6.5	k_2 oxygen.	k_3 hydrox.	k_4 dehyd.	–*p*-OHB	+*p*-OHB
WT	100 (44.0)	100 (5.7)	2.8×10^5	47	14	–163	–165
Y385F	2 (0.91)	6.5 (0.36)	3.2×10^5	1.8	>15	–163	–154
Y201F	3 (1.3)	7.5 (0.42)	3.0×10^5	0.04	nm	–169	–164
N300D	0.1	0.5 (0.06)	3.9×10^5	1.1	0.125	–180	–205

1991; Vervoort et al., 1992). Consistent with this proposal, the p*K* of *p*-OHB bound to wild-type PHBH is 7.4, significantly decreased from the solution value of 9.3, whereas in the absence of the hydrogen bond from Tyr201 (in the mutant Tyr201Phe) the p*K* of bound substrate is above pH 9 (Entsch et al., 1991). The efficiency (coupling) of hydroxylation, expressed as the percent yield of product based on consumption of NADPH, is also thought to correlate with the reactivity of substrates (Entsch et al., 1991). Only 5.9% of NADPH is utilized for the hydroxylation of *p*-OHB in reactions catalyzed by Tyr201Phe. This behavior is consistent with the role of Tyr201 in activating substrates by promoting ionization.

The structure of Tyr201Phe confirms that the effects of this mutation on the p*K* of bound *p*-OHB may be attributed to the loss of the hydrogen-bonding network involving substrate, Tyr201, and Tyr385, as disruption of the hydrogen-bond interactions at Tyr201 is a key difference between the wild-type and Phe201 mutant structures of oxidized PHBH complexed with *p*-OHB. From the structures, the hydroxyl group of Tyr385 appears to play an accessory role in the polarization of substrate and in the proton rearrangements involved in substrate ionization. The p*K*'s of the substrate analog, 4-hydroxycinnamate, bound to wild type and to the Tyr385Phe mutant have been measured to assess the contribution of the OH group of Tyr385 (Entsch et al., 1991) with the results suggesting only small effects of Tyr385 on substrate ionization. However, subsequent determinations of the p*K*'s of *p*-OHB and *p*-hydroxycinnamate bound to the mutant Asn300Asp (Palfey et al., 1994b) imply that *p*-hydroxycinnamate may not be the ideal analog for these studies.

An interesting property of the Tyr385Phe mutant is a loss of substrate specificity, shown by the ability of this mutant enzyme to hydroxylate 3,4-diOHB to form 3,4,5-trihydroxybenzoate (gallate) (Entsch et al., 1991). The Tyr201Phe mutant is also reported to hydroxylate 3,4-diOHB (Eschrich et al., 1993). Modeling of 3,4-diOHB, rotated to present its 5′-CH to the flavin 4a site in the active center of wild-type PHBH, reveals close contacts between the 3-OH of 3,4-diOHB and the 4-OH and 4-carbon atoms of Tyr201. Hydroxylation of 3,4-diOHB would seem to require shifts of the 201 side chain, even in the Tyr201Phe mutant. Presumably, loss of the interaction between Tyr201 and Tyr385 makes displacement of Tyr201 easier in the Tyr385Phe mutant, accounting for the loss of specificity observed in Tyr385Phe.

Structure–Function Correlations from Studies of the Mutant Asn300Asp. The salient properties of the Asn300Asp mutant are reported in the accompanying paper (Palfey et al., 1994b) and summarized in Table 5. Functional changes in this mutant are attributed to changes in electrostatic interactions and to atomic rearrangements, both of which perturb the electronic structure of the flavin [see Palfey et al. (1994b) for discussion]. Changes in the properties of the flavin are reflected in the potential for two-electron reduction of the PHBH–*p*-OHB complex, which decreases by 40 mV relative to wild type. The hydrogen-bonding network at Tyr201 and Tyr385 is retained in the Asn300Asp structure, with some changes in distances that separate donor and acceptor atoms (Table 4), but the p*K* of bound *p*-OHB is above pH 9. The rates of hydroxylation and of dehydration of the flavin 4a-OH (steps 3 and 4 of Scheme 1) are decreased by factors of 50 and 100. One of the striking observations is that the mutation dramatically decreases on/off rates for the binding of *p*-OHB to oxidized PHBH.

Rates of Substrate Binding and Conformational Equilibria in Asn300Asp. Analyses of accessibility show that substrates bound to PHBH are buried (Schreuder et al., 1988, 1989), so that substrate binding by PHBH must entail conformational changes. Recent studies of several mutants and ligand complexes of PHBH have revealed an additional mode of isoalloxazine binding by PHBH (Lah et al., 1993; H. A. Schreuder and A. Mattevi, unpublished). This flavin-binding mode may resemble an intermediate in the formation of

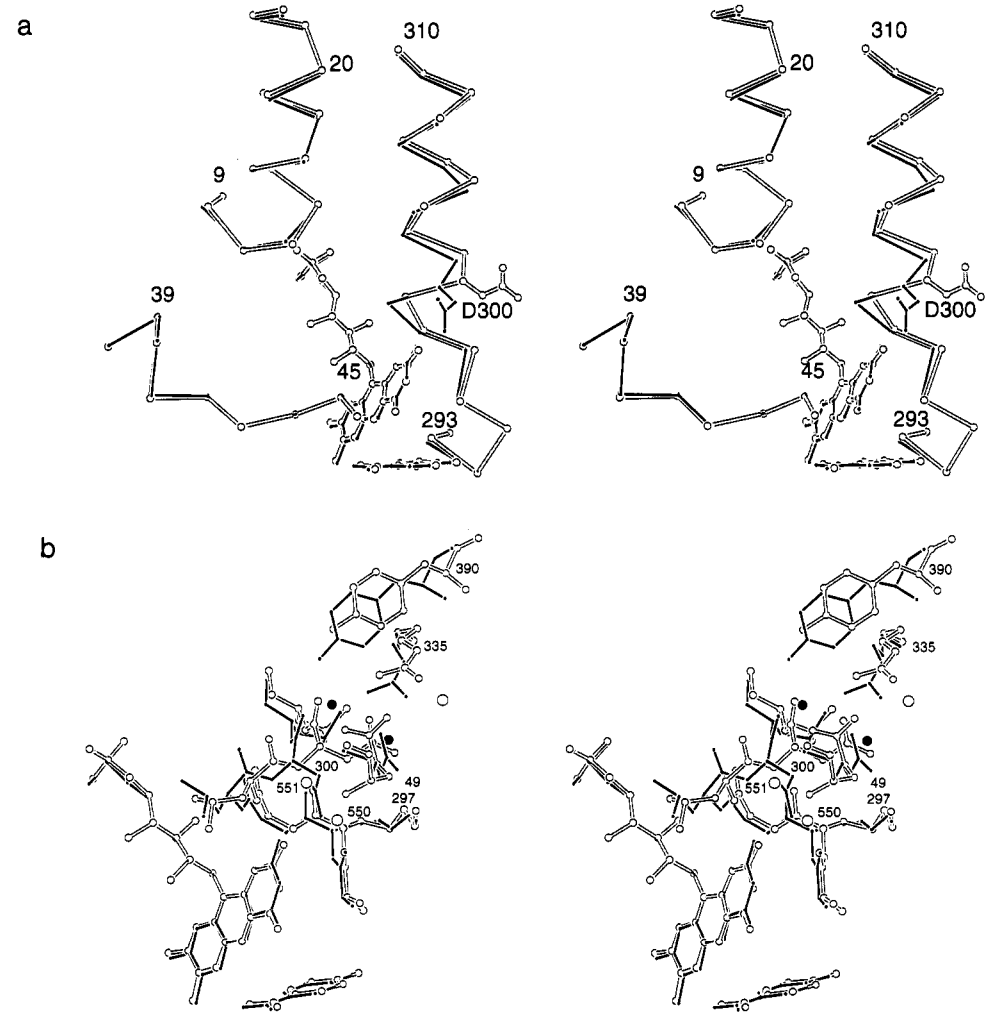

FIGURE 6: Structural changes in the mutant Asn300Asp. (a) An overview of the changes accompanying substitution of Asp for Asn at 300, showing shifts in the backbone Cα positions and in several side chains. The wild-type structure (thin bonds) was aligned with the mutant (thicker shaded bonds) by fitting the backbones of residues 1–175 (Kabsch, 1976). Substrate is seen edge-on below the flavin ring; FAD is truncated at the flavin phosphate. Displacements of the helix near the mutation site are evident in this view, as is the rearrangement of the side chain at residue 300. (b) A full atom representation from a vantage point similar to that of panel a, comparing the wild-type and Asn300Asp mutant structures. The mutant structure is drawn with thicker bonds; atoms from the wild-type structure are filled. Solvents 550 and 551 in the mutant replace the Asn300 side chain. Shifts of residues Glu49 and Arg335 are depicted, along with the loss of two waters (filled circles) from the wild-type structure and the addition of a new water (gray circle) near Glu49 in the mutant. The shape of the isoalloxazine ring is similar in wild-type and Asn300Asp structures.

substrate complexes. Substrate is bound in the usual fashion, but the flavin ring swings toward the molecular surface, losing its interactions with Asn300 and α-helix H10. In the alternative structure, solvent molecules occupy the pocket that binds the pyrimidine ring in the classic wild-type structures of PHBH–*p*-OHB. Mutations in the active center would be expected to affect the energetics and dynamics of ring displacements which may accompany substrate binding. However, it is not easy to relate the specific structural changes observed in the Asn300Asp mutant to the slow binding of substrate. Indeed, substitution of solvent bridges for direct interactions between the protein and the flavin ring might be expected to result in increased rather than decreased mobility of the flavin ring.

Electrostatic Effects. The pK of bound *p*-OHB is an indicator of the electrostatic interactions which stabilize the phenolate group relative to the un-ionized 4-OH. Increased pK's for *p*-OHB in both the Asn300Asp and Tyr201Phe mutants suggest that changes resulting from either mutation lead to lower electrostatic potentials near the substrate. The effects are mediated by different elements of the structure in the two different mutants: the disruption of the hydrogen-bond network in the tyrosine mutants, and the changes in other charge and dipole interactions in the Asn300Asp mutant. Because the Asp side chain in the mutant structure is 12 Å from the substrate 4-OH and occupies a position where its charge interacts with compensating charges, the charge on Asp300 may not be the dominant factor affecting substrate ionization in the Asn300 Asp mutant. Shifts of the helix dipoles (Hol et al., 1978; Aqvist et al., 1991; Quiocho et al., 1993), the incorporation of solvent, and other changes in nonbonded interactions can also produce significant changes in electrostatic interactions at the flavin ring and at the substrate atoms (Sharp & Honig, 1990). From the results of the individual mutations, it is not clear whether the changes in activity would be additive in double mutants like Tyr201Phe/Asn300Asp, but additivity is less likely when major structural rearrangements accompany the mutation (Carter et al., 1984; Wells et al., 1990).

ACKNOWLEDGMENT

The drawings of atomic models were prepared by Anita Metzger using the program MAXIM, written by Mark Rould.

We are grateful to Domenico Gatti for comments and discussions.

REFERENCES

Aqvist, J., Luecke, H., Quiocho, F. A., & Warshel, A. (1991) *Proc. Natl. Acad. Sci. U.S.A. 88*, 2026–2030.

Brünger, A. (1992) *X-PLOR, Version 3.1*, Yale University, New Haven, CT.

Brünger, A., Krukowski, A., & Erickson, J. W. (1990) *Acta Crystallogr. A46*, 585–593.

Cambillau, C., & Horjales, E. (1987) *J. Mol. Graphics 5*, 174–177.

Carter, P., Winter, G., Wilkinson, A. J., & Fersht, A. R. (1984) *Cell 38*, 835–840.

Entsch, B., & Ballou, D. P. (1989) *Biochim. Biophys. Acta 999*, 313–322.

Entsch, B., Ballou, D. P., & Massey, V. (1976) *J. Biol. Chem. 251*, 2550–2563.

Entsch, B., Palfey, B. A., Ballou, D. P., & Massey, V. (1991) *J. Biol. Chem. 266*, 17341–17349.

Eschrich, K., van der Bolt, F. J. T., de Kok, A., & van Berkel, W. J. H. (1993) *Eur. J. Biochem. 216*, 137–146.

He, J. J., & Quiocho, F. A. (1993) *Protein Sci. 2*, 1643–1647.

Hendrickson, W. A. (1985) *Methods Enzymol. 115*, 252–270.

Hol, W. G. J., van Duijnen, P. T., & Berendsen, H. J. C. (1978) *Nature 273*, 443–446.

Kabsch, W. (1976) *Acta Crystallogr. A32*, 922–923.

Lah, M. S., Gatti, D., Schreuder, H. A., Palfey, B. A., & Ludwig, M. L. *Flavins and Flavoproteins 1993* (Yagi, K., Ed.) Elsevier, Amsterdam (in press).

Palfey, B. A., Ballou, D. P., & Massey, V. (1994a) *Reactive Oxygen Species in Biochemistry II* (Valentine, J. S., Foote, C. S., Liebman, J., & Greenberg, A., Eds.) Chapman-Hall, London (in press).

Palfey, B. A., Entsch, B., Ballou, D. P., & Massey, V. (1994b) *Biochemistry* (preceding paper in this issue).

Schreuder, H. A., van der Laan, J. M., Hol, W. G. J., & Drenth, J. (1988) *J. Mol. Biol. 199*, 637–648.

Schreuder, H. A., Prick, P. A. J., Wierenga, R. K., Vriend, G., Wilson, K. S., Hol, W. G. J., & Drenth, J. (1989) *J. Mol. Biol. 208*, 679–696.

Schreuder, H. A., Hol, W. G. J., & Drenth, J. (1990) *Biochemistry 29*, 3101–3108.

Sharp, K., & Honig, B. (1990) *Annu. Rev. Biophys. Biophys. Chem. 19*, 301–332.

van Berkel, W. J. H., Westphal, A., Eschrich, K., Eppink, M., & de Kok, A. (1992) *Eur. J. Biochem. 210*, 411–419.

van der Laan, J. M., Swarte, M. B. A., Groendijk, H., Hol, W. G. J., & Drenth, J. (1989) *Eur. J. Biochem. 179*, 715–724.

Vervoort, J., van Berkel, W. J. H., Müller, F., & Moonen, C. T. W. (1991) *Eur. J. Biochem. 200*, 731–738.

Vervoort, J., Rietjens, M. C. M., van Berkel, J. H., & Veeger, C. (1992) *Eur. J. Biochem. 206*, 479–484.

Wells, J. A. (1990) *Biochemistry 29*, 8509–8517.

Wessiak, A., Schopfer, L. M., & Massey, V. (1984) *J. Biol. Chem. 12*, 12547–12556.

Wierenga, R. K., de Jong, R. J., Kalk, K. H., Hol, W. G. J., & Drenth, J. (1979) *J. Mol. Biol. 131*, 55–73.